Manuscript cover page

Effect of oxygen on degradation of defects on ta-C coatings deposited by filtered arc deposition

Motoyuki Murashima1*, Xingrui Deng1, Hiroto Izuoka1, Noritsugu Umehara1, Hiroyuki Kousaka1

Effect of oxygen on degradation of defects on ta-C coatings deposited by filtered arc deposition

Motoyuki Murashima[1]*, Xingrui Deng[1], Hiroto Izuoka[1], Noritsugu Umehara[1], Hiroyuki Kousaka[1]

[1]Department of Mechanical Science and Engineering, Graduate School of Engineering, Nagoya University

Furo-cho, Chikusa-ku, Nagoya, 464-8603, Japan

*Corresponding e-mail: motoyuki.murashima@mae.nagoya-u.ac.jp

Tel +81-52-789-2788, Fax +81-52-789-2788

Abstract

Among diamond-like carbon (DLC) coatings, tetrahedral amorphous carbon (ta-C) coatings show particularly high thermal stability and oxidation resistance due to their high sp^3 content and hydrogen-free structure. On the other hand, it is well known that high-temperature annealing leads to degradation of the ta-C structure, resulting in a release of stress, decrease of hardness, increase in surface roughness, and transformation of the coating nature. Although optical observation is a powerful candidate for imaging the surface conditions of ta-C coatings,

strong light emission due to high temperature prevents the acquisition of clear images. In this paper, we establish a novel in situ observation method using environment scanning electron microscopy (ESEM), which allows us to view ta-C surface defects and droplets at 650°C. A heater embedded in the ESEM increased the temperature on ta-C coatings to 650°C at gas pressure of 120 Pa. Using a variety of gas conditions including ambient air, dry nitrogen, or dry oxygen, we clarified the effect of the gases on the degradation of the defects. In a dry oxygen atmosphere, defects grew dramatically with annealing time, whereas nitrogen caused no significant transformation to ta-C surfaces. Raman spectroscopy analysis revealed significant structural change in one type of defect, while no noticeable Raman shift was detected in the other type. A focused ion beam created a cross-section of an annealed defect on the ta-C coating. Subsequently, energy dispersive X-ray spectroscopy (EDS) revealed the characteristics of defect growth; one type of defect was associated with a droplet on the interlayer, and the other with graphitization due to oxidization of ta-C on the droplets.

Keywords: ta-C coating, oxidation mechanism, surface defect, droplet, high temperature

1. Introduction

Diamond-like carbon (DLC) coatings have widespread applications as a protective coating because of their high hardness, low friction and wear resistance, and chemical inertness [1]. In some applications (e.g., piston rings [2] and pressing molds for glass lenses [3]), engineering coatings are subjected to a high-temperature environment, and thus many studies have attempted to improve the thermal stability of DLC coatings. For example, doping with other elements (e.g., nitrogen, boron or silicon) is one possible technique because dopants change the nature of DLC coatings, resulting in improved thermal stability as well as tribological, mechanical and optical properties [4,5].

For DLC coatings, oxidation resistance strongly depends on the nature of the coating in terms of hydrogen content and crystalline structure, as well as the sp^3/sp^2 ratio [6,7]. Hydrogenated amorphous carbon (a-C:H) is widely used in many industrial fields due to its ultra-low friction under some atmospheres [8], high wear resistance and high productivity. On the other hand, from the viewpoint of thermal stability, a-C:H starts to degrade at temperatures over 300°C due to hydrogen elimination [6,8].

a-C:H shows two types of degradation growth during the annealing process [9]. Raman analysis clarified that the a-C:H coatings began crystallizing and graphitizing transformation below 350°C, which was categorized as the first stage. In the second stage, at higher temperatures, the severe environment promoted a chemical reaction between oxygen and

carbon atoms, resulting in a decrease in film mass. Kulikovsky et al. investigated the effects of the degradation on the mechanical properties of DLC coatings [10]. The Raman spectra results, including G peak width and position, indicated that graphitization of DLC coatings proceeded as the annealing temperature increased.

In general, tetrahedral amorphous carbon (ta-C) coatings have better thermal stability due to their high sp^3 fraction and hydrogen-free structures [7,11]. The higher the sp^3 fraction of ta-C coatings, the better the thermal stability [11]. Previous research investigated the tribological properties of ta-C coatings at elevated temperatures (from room temperature to 500°C) [12,13]. Scanning electron microscope (SEM) observation after annealing tests showed many defects (1-10 μm in size) on the ta-C surfaces, and oxidization of defects at high temperature resulted in transformation of the nature of the coatings.

In the present paper, we clarify the defect degradation mechanism in an oxygen-containing environment at high temperature. We use an environmental scanning electron microscope (ESEM) with a chamber filled with dry oxygen gas to achieve in situ observation of ta-C surfaces with defects and droplets at high temperatures. The in situ observation method using ESEM enabled us to see ta-C surface conditions where optical observation was not possible at high temperature due to strong light emission. By varying the gas elements (i.e., ambient air, dry nitrogen, and dry oxygen), we were able to clarify the degradation mechanisms of defects and droplets on ta-C coatings.

2. Experimental methods

2.1 Specimen and annealing test

In this study, ta-C coatings were deposited on Inconel 750 substrates using the arc ion plating deposition method. In general, the high-energy arc discharge effectively ionizes carbon atoms from a carbon target, resulting in fine, dense ta-C coatings at a certain bias voltage. On the other hand, the arc scatters a few micrometer-sized carbon clusters, which finally grow into droplets. Here, filter cathode vacuum arcing (FCVA) deposition process was used to eliminate large droplets. However, even effective filtering methods are unable to remove droplets and defects completely, and therefore a few droplets and defects were observed as inhomogeneous surface topography [14]. We then observed the transformation of these defects (submicrons to micrometers in size) in different gas environments at high temperature.

The 0.7-μm thick ta-C coatings showed a hardness of 45 GPa (supplied by Nippon ITF Inc. (Japan) as HAX-DLC). Its coating processes and tribological properties are described elsewhere [13,15]. The hard ta-C coating had a high sp^3 fraction of 65%, which was determined based on the ratio of π-bonding (related to the diamond structure) to σ-bonding (related to the graphite structure) as quantified by electron energy-loss spectroscopy (EELS). The Inconel which was a Ni-Cr based alloy (Inconel X-750, Test materials, Japan) was

selected as a substrate because of its outstanding thermal stabilities. A chromium interlayer having about 30 nm thickness was deposited by electron cyclotron resonance (ECR) sputtering method (EIS-200ER Ion beam shower system, ELIONIX) with acceleration bias voltage of 2.0 kV. After the ta-C deposition, 3 mm × 3 mm specimens were cut (see Fig. 1a) and set on the heater embedded in the ESEM chamber (see Fig. 1b).

The schematic of ESEM and its mechanisms are described in Fig. 2. A gaseous secondary electron detector measures electrons derived by impact ionization through environment gas molecules. In the present research, we used acceleration voltage of 15 kV for the observation. The ESEM enables the observation of surface conditions even at temperatures so high that optical observation is not possible due to strong light emission. Before annealing tests, the ESEM chamber was vacuumed to a chamber pressure of 5.0×10^{-3} by a rotary pump. Then the introduced gas (i.e., ambient air, dry oxygen or dry nitrogen) increased the pressure to 120 Pa (after this gas introducing, the gas valves was closed). After that the heater increased the temperature of ta-C specimens from room temperature to 650°C over a period of 60 min, as shown in Fig. 3. The 650°C temperature was then maintained for 120, 70 or 90 min for ambient air, dry oxygen, and dry nitrogen tests, respectively. After the annealing tests, the heater was stopped, and the temperature decreased spontaneously.

Changing the gas element during the annealing tests highlighted the effect of the gas element on the degradation of ta-C coatings and defects at high temperature. Figure 4 is a

timing chart displaying the gas elements and temperature at each step. In the first step of the gas-changing test, the specimen temperature was increased to 650°C by the heater in dry oxygen at a pressure of 120 Pa. The specimen temperature was then maintained for 30 min. In the second step, dry nitrogen gas replaced the oxygen gas, and the pressure condition of 120 Pa was held for 45 min. Finally, dry oxygen gas replaced the nitrogen gas at 120 Pa.

ESEM images and Raman analysis were used to characterize the topology and the nature of ta-C coatings, respectively. The ESEM images were obtained at different temperatures to reveal the surface topography and transformation. Please note that the color in ESEM or SEM images represent the intensity of radiated electrons, rather than visible color changes in the samples themselves. The more gaseous secondary electrons derived by impact ionization through environment gas molecules increase, the more the involved areas in the ESEM images become whiter. Binarizing software translated the ESEM images to binary images consisting of white and black pixels, revealing the degradation growth at high temperature. Raman analysis characterized the nature of ta-C coatings and defects after annealing tests. The Raman analysis was performed using a laser wavelength of 535 nm and laser power of 1 mW, with a spot-size diameter of 1 μm.

2.2 Cross-sectional observation of defects

After the annealing tests, SEM and energy dispersive X-ray spectroscopy (EDS)

observation were conducted for cross-sections of defects on ta-C coatings. To create the cross-sections, we used a focused ion beam (FIB). The first step of the FIB process involved depositing a tungsten layer on the defects for protection (see Fig. 5). The protective layer was deposited by FIB-CVD, and covered the entire defect area to maintain the structures. For the second step, the FIB removed half of the defects, and in the third step, FE-SEM and EDS observations of the cross-sections were conducted to characterize the distribution of elements in the defects. For the observations, the stage was set at an oblique angle of 80 degrees.

3. Experimental results

3.1 In situ observation of defects at high temperature in various gas environments

Figure 6 shows the ESEM images of a ta-C surface before and after annealing in the ambient atmosphere (gas pressure of 120 Pa). After 120-min annealing, defect growths were clearly visible as expanding white circular areas. Sequential images revealed that there were two types of defect growth. The yellow and red circles in Fig. 6 enclose the different types of defect, which we define as type-1 and type-2, respectively.

Yellow circles (type-1 defects) indicate initially white points whose tone became brighter after annealing. The initially black defect area around white points turned white after 30-min annealing, and the size increased with annealing time. However, the brightest points at the center of the defect remained exactly the same size.

In contrast, the red circles (type-2 defects) enclose initially dark spots whose tone drastically changed to white after 30-min annealing. The white area expanded noticeably and the color brightened with increased annealing time, although the amount of expansion was less than that of type-1 defects. Interestingly, a comparable dark spot existed at the center of type-2 defects (see Fig. 6b-d).

The size of the degradation area on observed surfaces was calculated using binarized ESEM images. Figure 7 shows the evolution of the degradation area ratio in air, dry oxygen, and dry nitrogen atmosphere. In dry nitrogen, expansion of the degradation area was undetectable; in air and dry oxygen, the area increased with annealing time. Interestingly, both curves increased exponentially for at least 90 min of annealing. Collectively, the annealing test results confirm that oxygen gas strongly affects the degradation of defects on ta-C coatings.

We next conducted a gas-changing annealing test to clarify whether oxygen merely triggers the degradation or is actually required for the degradation to proceed. Figure 8 shows the evolution of the defect area at 650°C in a dry oxygen or nitrogen gas environment. In the first step with dry oxygen, the defect area increased with annealing time. Expansion of the defect area ceased, however, after dry nitrogen gas replaced the chamber gas. When dry oxygen gas was again introduced into the ESEM chamber, degradation began again. These results clearly reveal the effect of oxygen gas on degradation of ta-C, indicating that the chemical reaction

between reactive gas and carbonaceous defects (e.g., droplets) is the primary reason for defect growth.

3.2 Cross-sectional observation of defects

Raman analysis characterized the nature of defects before and after annealing with/without defects. For as-deposited ta-C areas without any defects, the I_D/I_G ratio and G peak position were 0.17 and 1559 cm^{-1}, respectively. These values were in good accord with previous research using a similar laser wavelength [16].

Other Raman curves (i.e., normal area, type-1 defect and type-2 defect) was measured from the tested sample of 120-min annealing in ambient air. The D peak for the type-1 defect increased slightly after annealing, whereas there was no significant change in the curve. In contrast, the D peak for the type-2 defect increased drastically (see Fig. 9). Because ta-C coatings generally have high thermal stability due to their high sp^3 fraction, the nature of the type-1 defect was suggested to be similar in structure to normal ta-C. On the other hand, many studies using Raman analysis for DLC coatings have shown that an increase in the D peak results in a higher I_D/I_G ratio, corresponding to an increase of sp^2 structures and clustering of graphite-like structures [13,16]. In the present study, the Raman spectrum change in type-2 defect areas after annealing seems to indicate transformation of the atomic nature of the defect.

FE-SEM and EDS observations of FIB-cut specimens revealed topological changes and element distribution in both types of defect. Figure 10 shows the cross-section image and element distribution of the type-1 defect. The tungsten layer covering the defect prevented unnecessary damage from the FIB process. In the FE-SEM image, the tungsten layer appears almost white, due to its high atomic weight. Interestingly, the image shows the defect as a dome-like structure with a chromium core at the center (see the EDS elemental map for chromium in Fig. 10). The EDS mapping clarified that the dome consisted of carbonaceous structures.

FE-SEM observations for the type-2 defect showed a different topography than the type-1 defect. There was no dome structure on the surface (see Fig. 11). The EDS mapping showed that spread chromium existed between the tungsten layer and the substrate, and no carbonaceous structure existed in the area. These results suggested that a thin ta-C layer remained, because the Raman analysis in Fig. 9 indicated the existence of ta-C coating or a transformed carbonaceous structure.

4. Mechanism of defect growth at high temperature in oxygen gas environment

In this section, we discuss the growth mechanism of the type-1 defect first. A series of experiments consisting of annealing tests in the ESEM, Raman, FE-SEM and EDS analysis revealed the characteristics of the type-1 defect. These included the expansion of degradation

area with annealing time, the thermal stability indicated by the Raman analysis, and the existence of the chromium core and carbonaceous dome. More important was the finding that oxygen starts and accelerates the degradation. Together, these results showed that oxidation plays an important role at the interface between a ta-C coating and interlayer.

Oxidization of defects can occur at the interface between a chromium interlayer and a ta-C coating due to increased chemical reactivity with temperature. Previous studies revealed the high reactivity of the surface structure compared to bulk material [11]. Oxygen can enter the interface through atomic gaps created by the non-uniformity in ta-C coatings due to chromium droplets. Subsequently, the chemical reaction results in poor adhesion between the ta-C and chromium interlayer, and finally tiny delaminations and occur. The delamination exposes a new interface because of the high internal stress in ta-C coatings [17], resulting in expansion of the degradation area. Because the delaminations could occur in nano/atomic scale, even the FE-SEM observations (see Fig. 10 and Fig. 11) was not able to find clear images. On the other hand, atomic force microscopy (AFM) images displayed that some dome-shaped defects had a hole on the center of them (see Fig. 12). This kind of cracks/delaminations should be the trigger of above-mentioned defect growth mechanisms.

From the viewpoint of surface topography, the dome shape defects show good agreement with previous research results that found increased surface roughness on a-C coatings with temperature [9]. The dome-shaped ta-C with the chromium core observed in this study and its

expansion are the likely origin of the increase in surface roughness, the mechanism of which has been unclear due to the lack of micro/sub-micron-order observations for defects with SEM.

Thermal expansion mismatch between the ta-C coating and the interlayer is another possible cause of ta-C delamination. However, the annealing test results in dry nitrogen clarified that thermal expansion mismatch was not able to start the degradation. Moreover, the gas-changing test demonstrated that thermal expansion mismatch could not accelerate the degradation. We cannot conclude here that thermal expansion mismatch plays no role in ta-C delamination, because annealing usually increases both thermal expansion mismatch and chemical reactivity. However, the increase in mismatch and increase in chemical reactivity happen simultaneously in real engineering components, and thus the present work provides important insights despite its limitations.

In the case of the type-2 defect, oxygen also plays an important role in the defect degradation. There is a very large body of research demonstrating that DLC coatings with high sp^3 fraction prevent structural transformation (e.g., graphitization and oxidization) [18,19]. Some defects (i.e., high sp^2 fraction areas and droplets mainly composed of sp^2 structures [3]) readily react chemically with oxygen, resulting in changes in the nature of the defects that can be observed in the Raman spectrum (see Fig. 9). Reacted atoms in the droplets can evaporate as carbon oxide or carbon dioxide, resulting in reduced coating

thickness. Figure 10 and 11 reveals that the thickness of 120-min annealed ta-C coating was about 0.17 μm. Consequently, the etching rate of the ta-C coating was calculated to be 4 nm/min under 650ºC annealing in oxygen. Because the evaporation should also occur inside of the dome-shape defect, the reduction promotes the cracks/delaminations growth in the type-1 defect. Figure 11 showed that the spread chromium covered the substrate. The distorted topology could prevent coating uniformity, resulting in unstable carbonaceous structures, larger surface area and discontinuous internal stress. The unstable coating could change its structure easily and show higher etching rate, resulting in very thin remained coating detected by the Raman analysis.

Although ta-C coatings are relatively thermally stable, the presence of defects can limit the operating temperature or environment. FCVA coating methods remove droplets nicely compared to other PVD methods, although even FCVA is not able to filter all droplets and remove defects completely [14]. Furthermore, interlayer droplets can cause a poor coating quality because of a reduction in adhesion, non-uniformity of coatings and discontinuous stress distributions. Many studies have clarified the thermal stability of DLC coatings, especially that of ta-C, and quite a few have focused on the poor thermal stability of defects and droplets on ta-C coatings [13]. The present results indicate that non-uniformity of coatings results from carbonaceous droplets, interlayer droplets, and sp^2 distribution, triggering degradation of ta-C coatings. Figure 13 is a FE-SEM image showing droplets

before an annealing test. The appearance can be the type-2 defect, and displays the non-uniformity above discussed, resulting in a poor coating quality. Furthermore, the carbonaceous coatings on the defect react easily due to larger surface area which can accelerates an etching speed. Consequently, the thin coating remained, resulting in the Raman analysis, FE-SEM and EDS observations (see Fig. 8 and Fig. 11).

Comparing the present research results to previous reported results [13], we can estimate the effect of a gas pressure on a degradation speed. In the present research work, the grown defect size annealed in ambient air with temperature of 500ºC for 50 minutes was around 7.5 μm. In spite of the longer annealing time (120 minutes) in the present research, the maximum defect size was approximately 7.2 μm. The difference of gas pressure (120 Pa in the present research, and atmospheric pressure in the referred research) can affect the degradation speed. Higher gas pressure should increase the amount of oxygen molecules involving degradation reaction, and then the reaction speed can accelerate. The relation between gas pressure (amount of oxygen molecules) and degradation speed is an important future work.

Conclusions

This study revealed the degradation mechanisms of defects on ta-C coatings at high temperature using a novel in situ observation method with ESEM. The clear images obtained with ESEM showed the growth of defects at a high temperature of 650°C, a condition under

which optical observation is not possible due to strong light emission.

Systematic experiments revealed the important role of oxygen in ta-C degradation. In contrast, we also clarified that nitrogen gas, which is a common inert gas, was unable to start the degradation of ta-C coatings. Moreover, the gas-changing test showed that the absence of oxygen stopped the degradation process even after it had already begun.

Our present research found two types of defect growth mechanisms at high temperature for ta-C coatings manufactured by the FCVA method. The first type (classified type-1 defect) involved an interlayer droplet resulting in ta-C delamination and a dome-shaped structure. The second type (type-2 defect) occurred due to transformation and/or evaporation of the carbonaceous structure, which was confirmed by Raman analysis.

References

1. J. Robertson, Diamond-like amorphous carbon, Mater. Sci. and Eng. R: Reports, 37 (2002) 129-281.

2. S.C. Tung, H. Gao, Tribological characteristics and surface interaction between piston ring coatings and bled of energy-conserving oils and ethanol fuels, Wear, 255 (2003) 1276-1285.

3. H. U. Kim, S. H. Jeong, H. J. Kim, J. H. Kim, Optical properties of aspheric glass lens using DLC coating mold, Key Eng. Mater., 345-346 (2007) 1577-1580.

4. S.C. Ray, G. Bhatttacharya, M.A. Miller, S. Sarma, R.K. Upadhay, J.A. McLaughhlin, S.S. Roy, A facile method for the deposition of thermally stable diamond like carbon thin films via carbon dioxide precursor gas, Diam. and Relat. Mater., 73, (2017) 93-98.

5. C. Donnet, Recent progress on the tribology of doped diamond-like and carbon alloy coatings: a review, Surf. and Coat. Technol., 100-101 (1998) 180-186.

6. G. Gassner, P. H. Mayrhofer, J. Patscheider, C. Mitterer, Thermal stability of nanocomposite CrC/a-C:H thin films, Thin Solid Films, 515 (2007) 5411-5417.

7. R. Kalish, Y. Lifshitz, K. Nugent, S. Prawer, Thermal stability and relaxation in diamond-like-carbon. A Raman study of films with different sp3 fractions(ta-C to a-C), Appl. Phys. Lett., 74 (1999) 2936-2938.

8. A. Vanhulsel, B. Blanpain, J.-P. Celis, J. Roos, E. Dekempeneer, J. Smeets, Study of the wear behavior of diamond-like coatings at elevated temperatures, Surf. and Coat. Technol., 98 (1998) 1047-1052.

9. D. Y. Wang, C. L. Chang, W. Y. Ho, Oxidation behavior of diamond-like carbon films, Surf. and Coat. Technol., 120-121 (1999) 138-144.

10. V. Kulikovsky, V. Vorlicek, P. Bohac, A. Kurdyumov, A. Deyneka, L. Jastrabik, Thermal stability of microhardness and internal stress of hard a-C films with predominantly sp^2 bonds, Diam. and Relat. Mater., 12 (2003) 1378-1387.

11. M. Rouhani, F. C. N. Hong, Y. R. Jeng, In-situ thermal stability analysis of amorphous carbon films with different sp^3 content, Carbon, 130 (2018) 401-409.

12. X. Deng, H. Kousaka, T. Tokoroyama, N. Umehara, Thermal stability and high-temperature tribological properties of a-C:H and Si-DLC deposited by microwave sheath voltage combination plasma, Tribol. Online, 8 (2013) pp. 257-264.

13. X. Deng, K. Hiroyuki, T. Tokoroyama, N. Umehara, Tribological behaviors of tetrahedral amorphous carbon (ta-C) coatings at elevated temperature, Tribol. Int., 75 (2014) 98-103.

14. A. Leson, G. Englberger, D. Hammer, S. Makowski, C.-F. Meyer, M. Leonhard, H.-J. Scheibe, V. Weihnacht, Diamond-like carbon thin films enhance efficiency – laser arc deposition of ta-C, Vakuum, 27 (2015) 24-28.

15. Koji Miyake, Characteristics and applications of diamond like carbon (DLC) films, J. Vac. Soc. Jpn., 60, (1017) 428-436.

16. A.C. Ferrari, B. Kleinsorge, N.A. Morrison, A. Hart, V. Stolojan, J. Robertson, Stress reduction and bond stability during thermal annealing of tetrahedral amorphous carbon, J. Appl. Phys., 85 (1999) 7191-7197.

17. V. Kulikovsky, P. Bohac, F. Franc, D. Chvostova, A. Deineka, V. Vorlicek, L. Jastrabik, Degradation and stress evolution in a-C, a-C:H and Ti-C:H films, Surf. and Coat. Technol., 142-144 (2001) 702-706.

18. S. Bhowmick, A. Banerji, M.Z.U. Khan, M.J. Lukitsch, A.T. Alpas, High temperature tribological behavior of tetrahedral amorphous carbon (ta-C) and fluorinated ta-C coatings against aluminum alloys, Surf. and Coat. Technol., 284 (2015) 14-25.

19. H. Nakazawa, T. Mikami, Y. Enta, M. Suemitsu, M. Mashita, Structure, chemical bonding and these thermal stabilities of diamond-like carbon (DLC) films by RF magnetron sputtering, Jpn. J. Appl. Phys., 42 (2003) 676-679.

Figure captions

Fig. 1 Photo images of: (a) a ta-C coated sample; and (b) the heater embedded in the ESEM

Fig. 2 Schematic image of environmental scanning electron microscope. GSED stands for gaseous secondary electron detector.

Fig. 3 Annealing process in air, dry oxygen, or dry nitrogen gas

Fig. 4 Annealing process in environment gas-change tests with dry oxygen, dry nitrogen, and dry oxygen gas in the 1^{st}, 2^{nd}, and 3^{rd} steps, respectively

Fig. 5 Schematics of FIB cut processes and FE-SEM observation for a cross section of a defect

Fig. 6 ESEM images on ta-C coating during annealing in air atmosphere after: (a) 0 min; (b) 30 min; (c) 90 min; and (d) 120 min

Fig. 7 Evolution of the degradation area ratio of ta-C coating annealed in air, dry oxygen, and dry nitrogen. A_d and A_0 indicate total defect area during annealing tests and before the tests, respectively.

Fig. 8 The results of the gas-change test for clarifying the effect of oxygen on the degradation area of ta-C coating during annealing

Fig. 9 Raman spectrum of as-deposited and three different areas after 120-min annealing in ambient air

Fig. 10 FE-SEM and EDS mapping of type-1 defect after annealing in oxygen

Fig. 11 FE-SEM and EDS mapping of type-2 defect after annealing in oxygen

Fig. 12 ta-C surface profiles (a) before/(b) after annealing measured by AFM

Fig. 13 FE-SEM image of droplets on ta-C coating before annealing

Figures

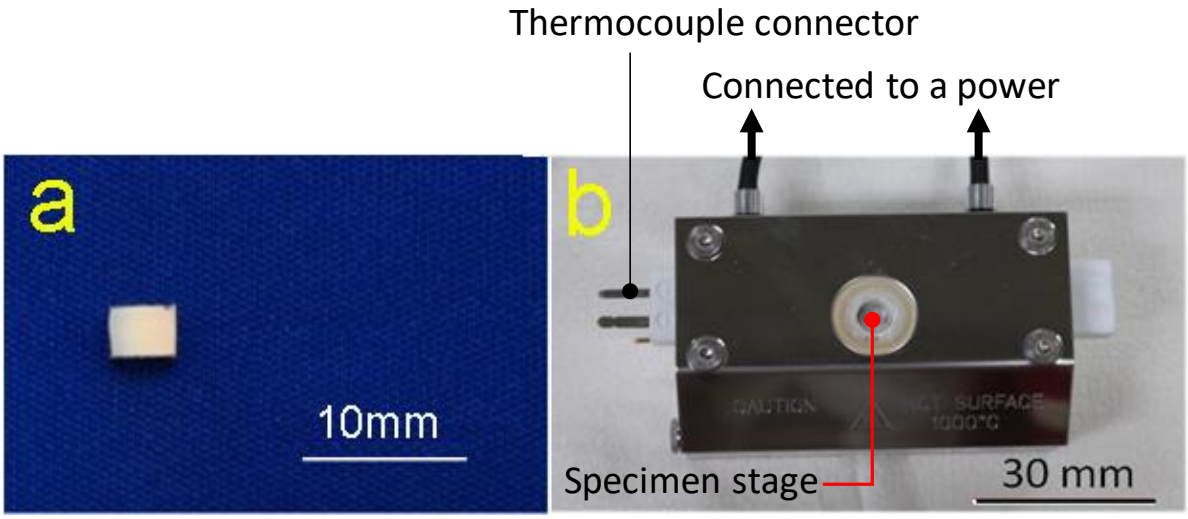

Fig. 1

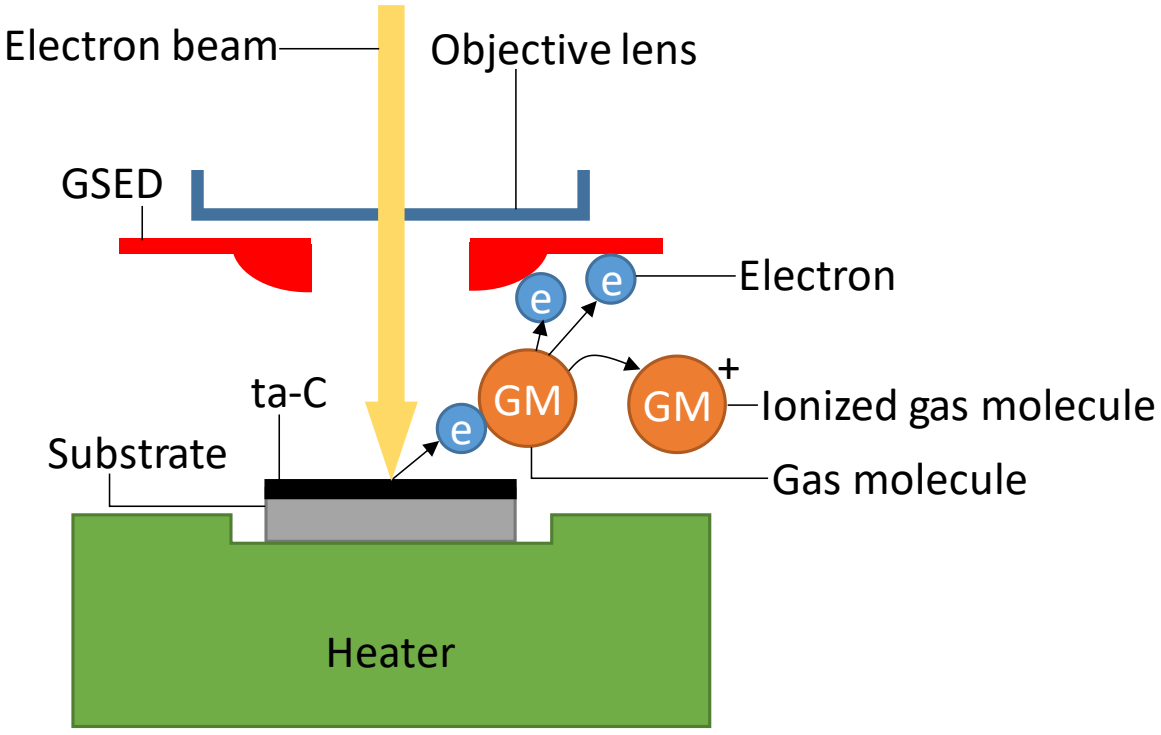

Fig. 2

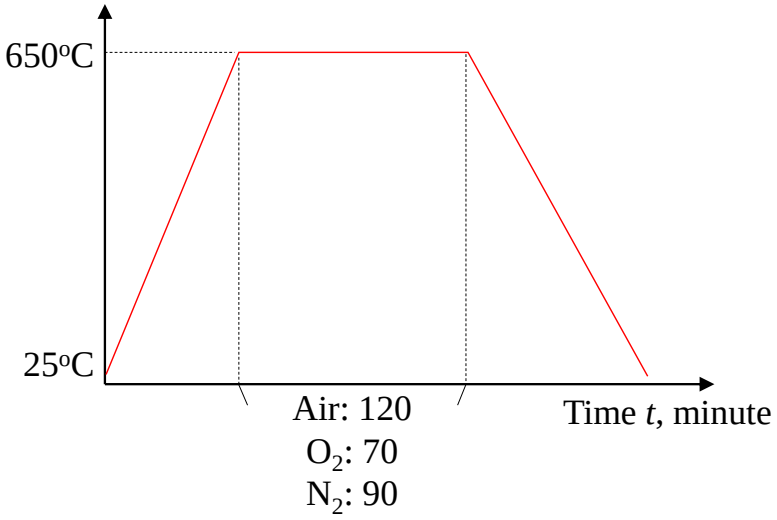
650°C
25°C
Air: 120
O2: 70
N2: 90
Time t, minute

Fig. 3

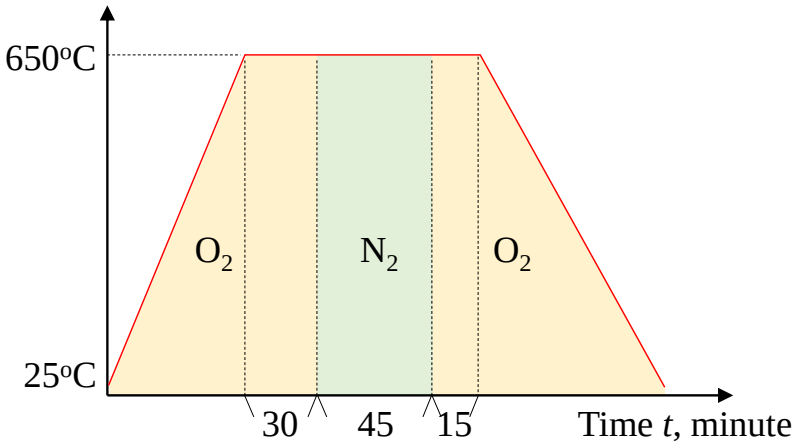
650°C
25°C
O2
N2
O2
30
45
15
Time t, minute

Fig. 4

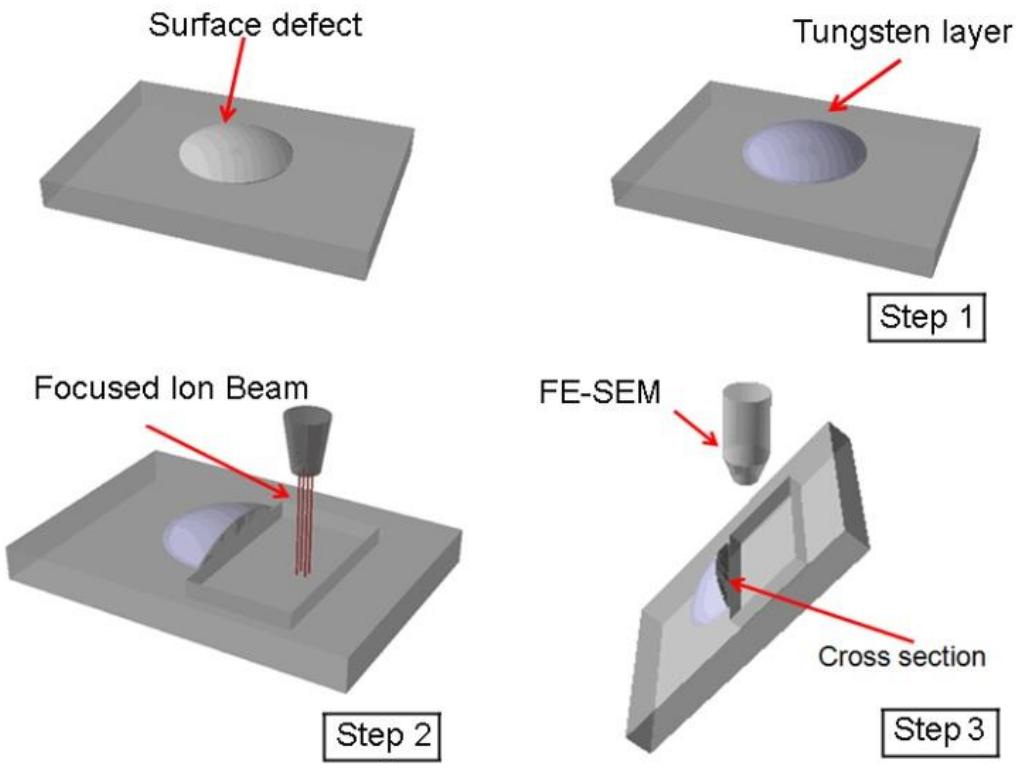
Surface defect
Tungsten layer
Step 1
Focused Ion Beam
Step 2
FE-SEM
Cross section
Step 3

Fig. 5

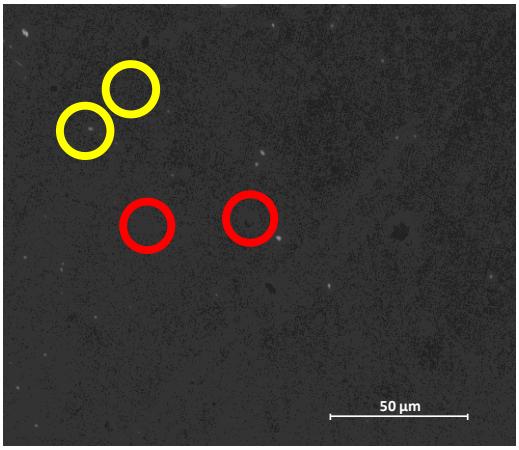

(a) 0 min

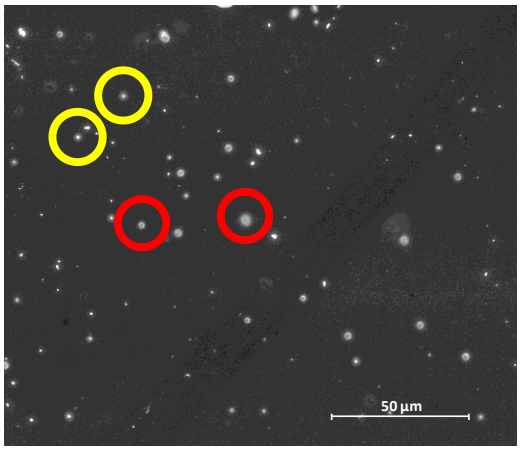

(b) 30 min

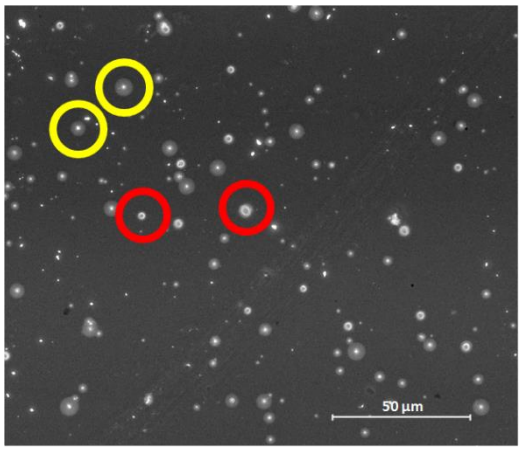

(a) 90 min

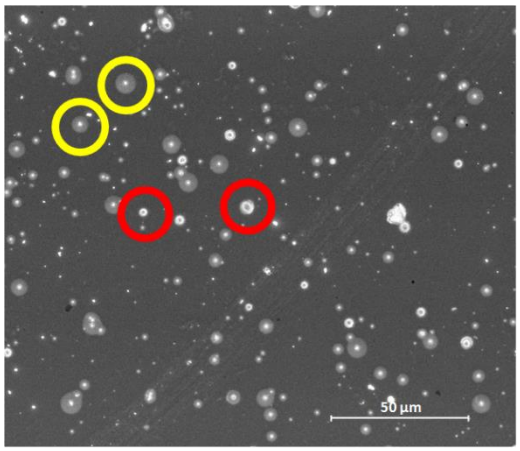

(b) 120 min

Fig. 6

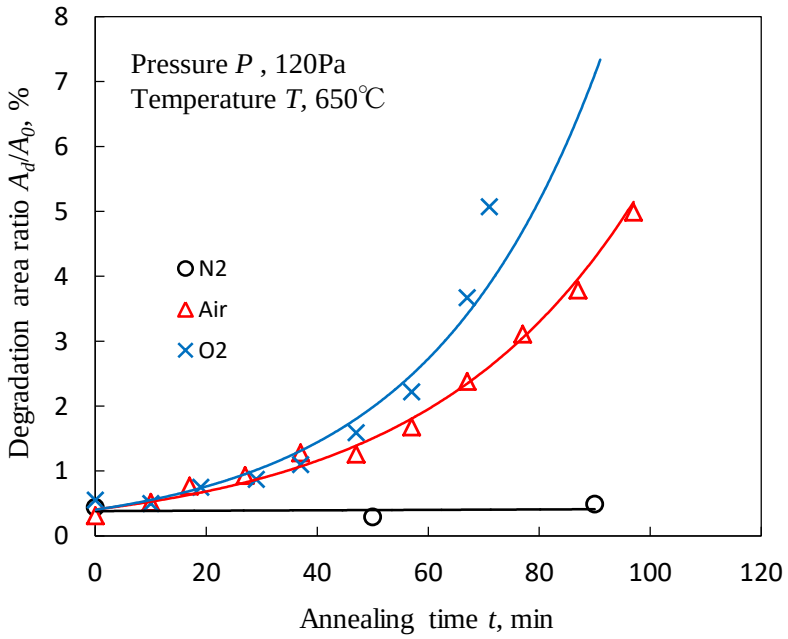
Pressure P , 120Pa
Temperature T, 650℃
N2
Air
O2
Degradation area ratio A_d/A_0, %
Annealing time t, min
0
1
2
3
4
5
6
7
8
0
20
40
60
80
100
120

Fig. 7

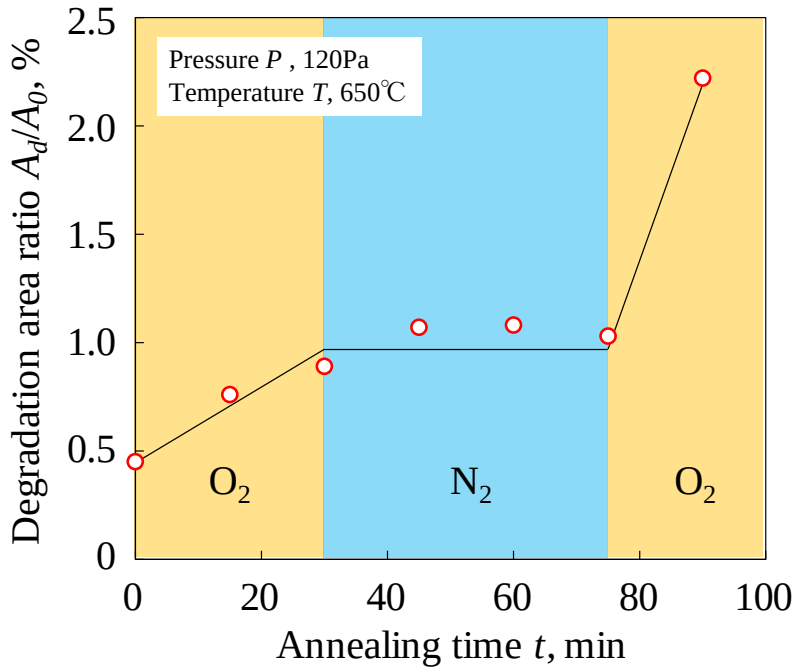
Pressure P , 120Pa
Temperature T, 650℃
O_2
N_2
O_2
Degradation area ratio A_d/A_0, %
Annealing time t, min
0
0.5
1.0
1.5
2.0
2.5
0
20
40
60
80
100

Fig. 8

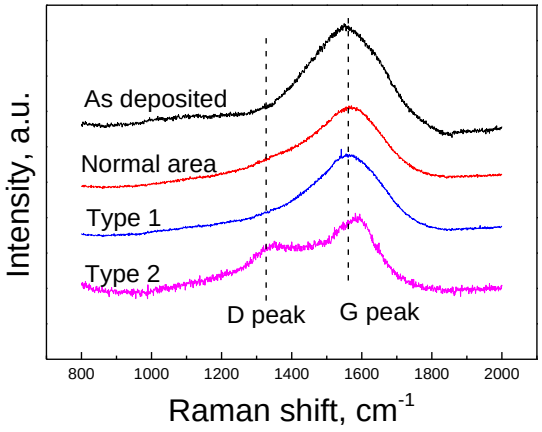
As deposited
Normal area
Type 1
Type 2
D peak
G peak
Intensity, a.u.
800
1000
1200
1400
1600
1800
2000
Raman shift, cm-1

Fig. 9

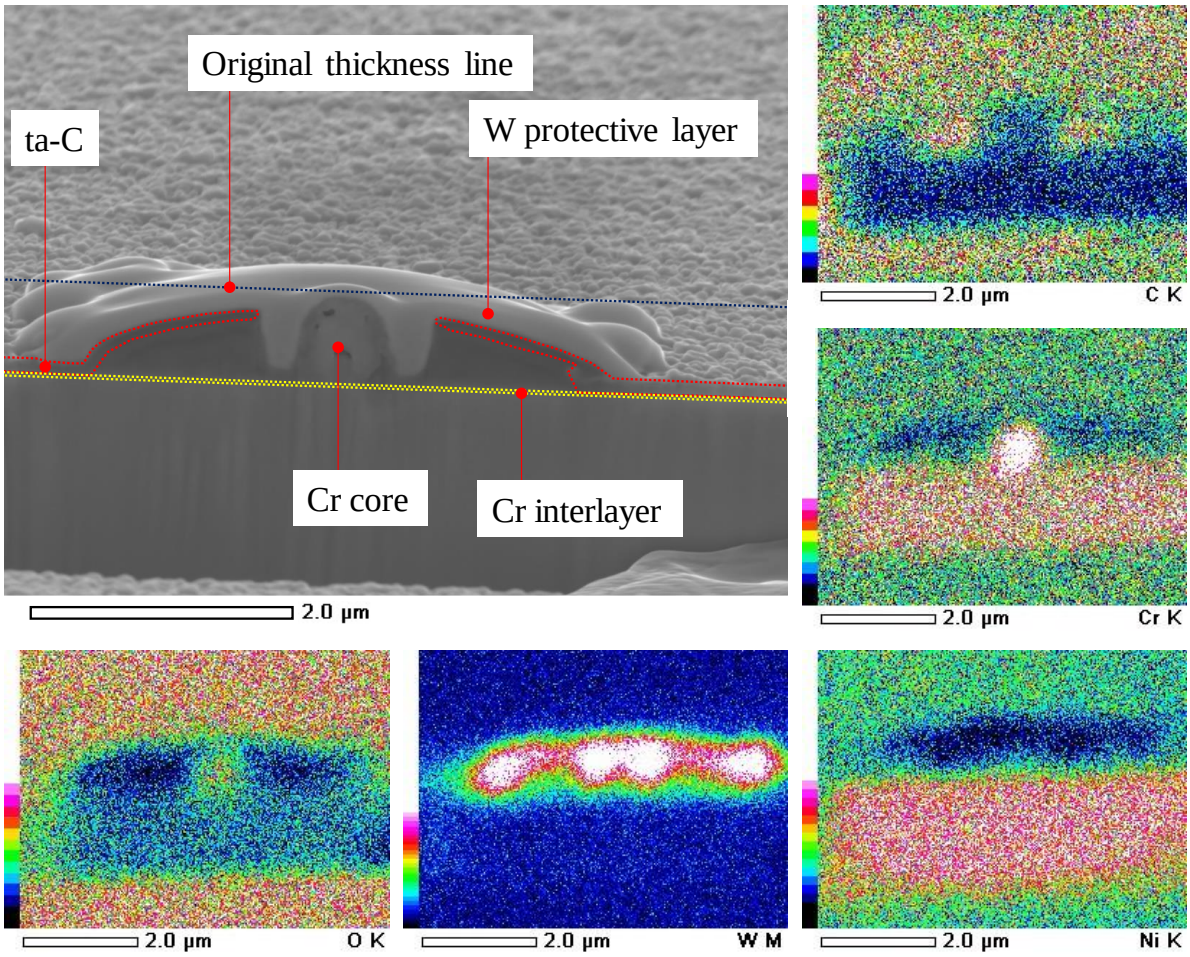
Original thickness line
ta-C
W protective layer
Cr core
Cr interlayer
2.0 μm
2.0 μm
C K
2.0 μm
Cr K
2.0 μm
O K
2.0 μm
W M
2.0 μm
Ni K

Fig. 10

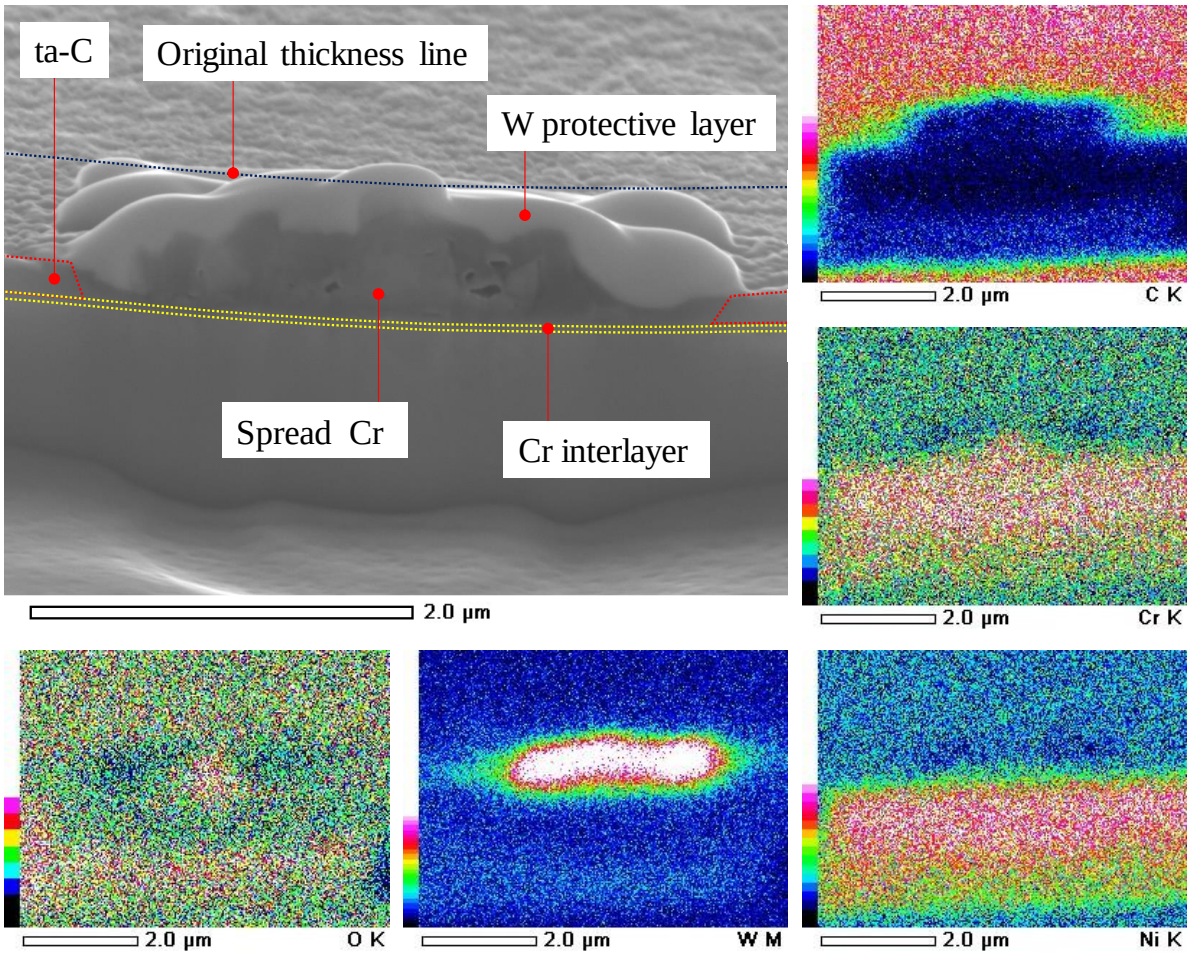
ta-C
Original thickness line
W protective layer
Spread Cr
Cr interlayer
2.0 µm
2.0 µm
C K
2.0 µm
Cr K
2.0 µm
O K
2.0 µm
W M
2.0 µm
Ni K

Fig. 11

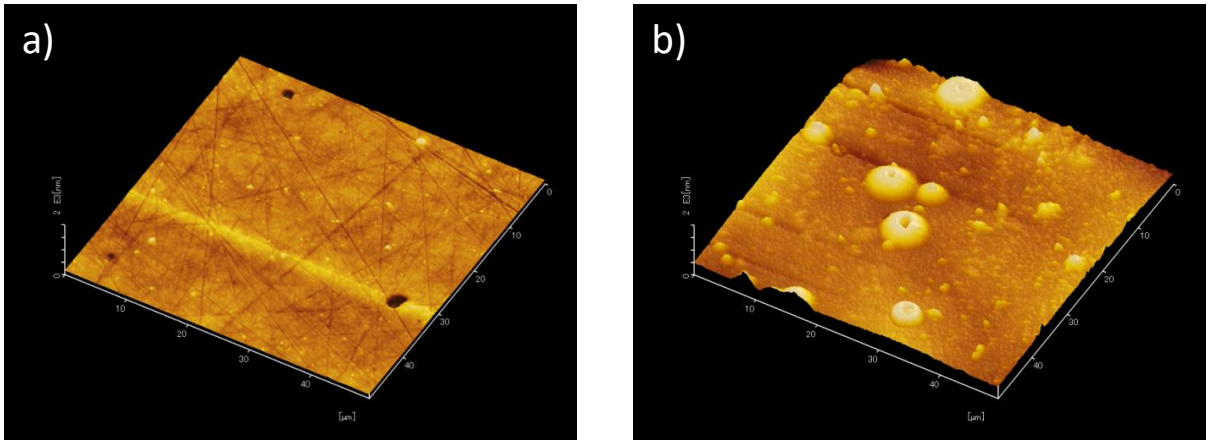
a)
b)

Fig. 12

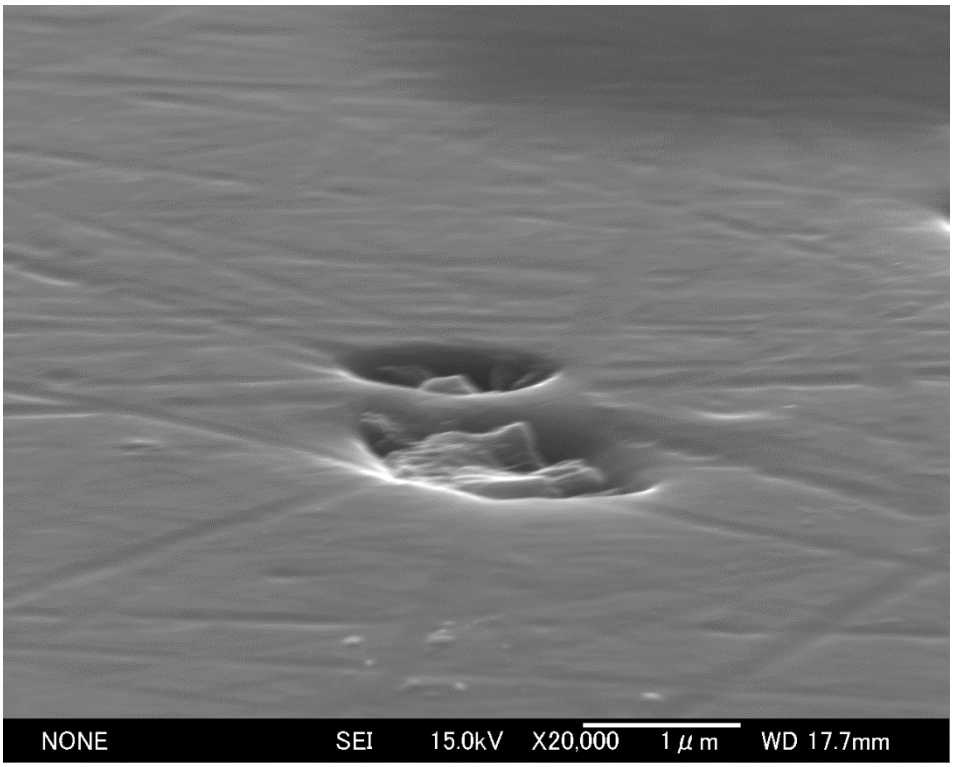

Fig. 13